NANO LETTERS

2008
Vol. 8, No. 5
1335-1340

Strain-Driven Electronic Band Structure Modulation of Si Nanowires

Ki-Ha Hong,* Jongseob Kim, Sung-Hoon Lee, and Jai Kwang Shin

Samsung Advanced Institute of Technology, Mt. 14-1, Nongseo-Dong, Giheung-Gu, Yongin-Si, Gyeonggi-Do, 446-712, Korea

Received December 31, 2007; Revised Manuscript Received March 14, 2008

ABSTRACT

One of the major challenges toward Si nanowire (SiNW) based photonic devices is controlling the electronic band structure of the Si nanowire to obtain a direct band gap. Here, we present a new strategy for controlling the electronic band structure of Si nanowires. Our method is attributed to the band structure modulation driven by uniaxial strain. We show that the band structure modulation with lattice strain is strongly dependent on the crystal orientation and diameter of SiNWs. In the case of [100] and [111] SiNWs, tensile strain enhances the direct band gap characteristic, whereas compressive strain attenuates it. [110] SiNWs have a different strain dependence in that both compressive and tensile strain make SiNWs exhibit an indirect band gap. We discuss the origin of this strain dependence based on the band features of bulk silicon and the wave functions of SiNWs. These results could be helpful for band structure engineering and analysis of SiNWs in nanoscale devices.

Silicon nanowires (SiNWs) have been considered as one of the most manufacturable nanostructured building blocks. The prototype SiNW devices such as nanowire-based field effect transistors,[1,2] photodetectors,[3] and biosensors[4] have been reported. While most devices using SiNWs are obtained through bottom-up approaches,[5,6] it is recently reported that a less than 10 nm sized Si nanowire MOSFET was successfully fabricated using conventional top-down CMOS technology.[7] This means that the geometry and crystallography of SiNWs can be precisely controlled with conventional processing methods as well as bottom-up processes. Thus, the processability and quantum effects of SiNWs encourage research in the field of nanoscale electronic and photonic devices.[7–10]

Various types of silicon photonic devices have been investigated because silicon has merits in cost and processability,[11–14] although the usage of the bulk silicon is limited due to its indirect and small band gap feature. Si nanocrystals and nanowires are expected to have a wide band gap due to quantum confinement and exhibit a direct band gap characteristic due to zone folding to the Γ-point. It has been reported that nanometer sized Si nanocrystals[15] and nanowires[16,17] can show blue-shift photoluminescence (PL). Guichard et al. emphasized that SiNWs have advantages over silicon nanocrystals in that the devices using nanocrystals exhibit oxide wearout during charge injection and have limitations in reliability[18,19] and these issues can be circumvented in the nanowire devices because charge can be injected directly into the wire at both ends without traversing an oxide.[17] Therefore, we expect that silicon nanowires can be low-cost materials for nanophotonic device technologies compatible with conventional silicon technologies.

There are several reports showing light emissions from the SiNWs.[20–22] However, light emssion from direct band gap in SiNWs has not been demonstrated yet although many theoretical investigations predict that SiNWs can have wide and direct band gaps.[23–25] Several reasons can be addressed based on the band structure of SiNWs. The diameters of SiNWs grown with catalytic method are often too large to have a direct band gap. While SiNWs of diameter less than 10 nm grow primarily in the [110] direction during vapor−liquid−solid methods,[5,26,27] it has been reported that [110] SiNWs may not be efficient for light emitting due to the relatively small density of states (DOS) of the conduction band at the Γ-point.[25] Moreover, higher index SiNWs such as [111] and [11$\bar{2}$] have an indirect band gap.[25] Even in the case of [100] SiNWs, the energy difference between direct band gap and indirect band gap is relatively small and the DOS of the indirect band is larger than that of the direct band. Therefore, the modification of SiNWs band structure is necessary in order to enhance the direct band gap characteristic for efficient nanophotonic devices.

Lattice strain is a useful method for modulating band structures. In designing electronic devices, it has been widely studied to enhance the device performance by modifying the band structure of silicon.[28–30] Applying strain is a very economical way for improving the performance of devices and has the advantage of being compatible with conventional CMOS processes for device fabrication. Recently, there were a few attempts to tailor the optical properties of SiNWs

* Corresponding author. E-mail: kiha.hong@samsung.com. Telephone: +82-31-280-9169. Fax: +82-31-280-9308.

10.1021/nl0734140 CCC: $40.75
Published on Web 04/11/2008

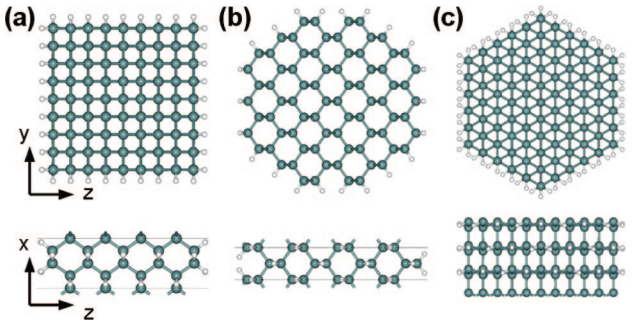

Figure 1. Structures of Si nanowires. (a) [100] SiNW with the effective diameter of 2.2 nm. (b) [110] SiNW with the effective diameter of 2.2 nm. (c) [111] SiNW with the effective diameter of 2.1 nm. We determine the effective diameter of the SiNWs by calculating the diameter of the circular shape with the same area as each nanowire.

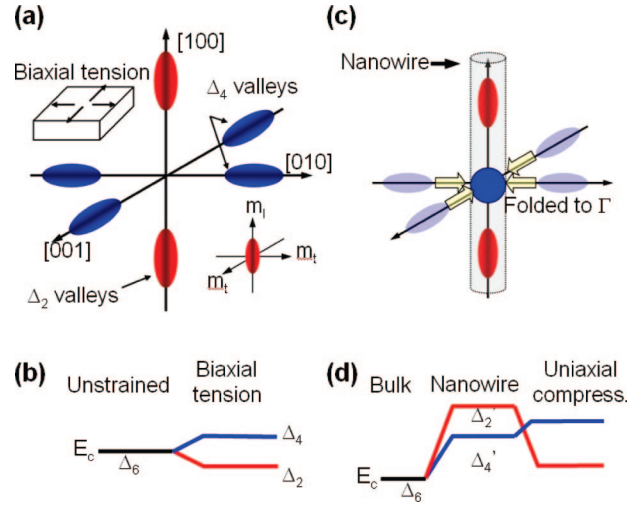

Figure 2. (a) Iso-energy surfaces in energy vs k-vector ($E-k$) diagram of conduction band of bulk silicon. Six lobes are formed near X-point. These lobes have ellipsoidal shape with two light transverse mass (m_t) and a heavy longitudinal mass (m_l). (b) Biaxial tension on bulk Si splits the 6-fold degenerate valleys of the conduction band into 2-fold (out-of-plane) and 4-fold (in-plane) degenerate valleys, lowering the energy level of the 2-fold degenerate valleys. (c) Schematic feature of $E-k$ diagram of SiNW. Lobes in confined plane are folded into the Γ-point. (d) Energy level splitting of 6-fold degenerate bands in [100] SiNWs into Δ_4' and Δ_2' valleys due to quantum confinement and their variation under uniaxial compressive strain.

through strain,[22,31] but the contributions of the strain on the band structure of SiNWs has not been clearly analyzed yet. Here, we report the electronic band structures of SiNWs and the dependence of those on the lattice strain, and it is presented that the lattice strain can be a new strategy for SiNWs to have a direct band gap.

Density functional theory (DFT), as implemented in the VASP program package,[32] with a plane wave basis expansion and an energy cutoff of 240 eV, are used. The core−valence interaction is described by the projector-augmented wave (PAW) method,[33] and the generalized gradient approximation (GGA) is used with the PW91 exchange-correlation functional. The distance between neighboring wires should be greater than 10 Å in order to reduce the cell to cell interaction. We first obtained the bulk Si structure applying Monkhorst−Pack sampling with a $4 \times 4 \times 4$ k-point grid and then constructed a nanowire supercell with the resulting lattice constant and a $1 \times 1 \times 4$ k-point grid. We fully optimized the atomic configurations and the lattice constant of SiNWs along the wire axis. We will discuss the characteristics of electronic band structures using wave function analysis, obtained with the SIESTA code.[34]

The uniaxial lattice strain is given by changing the unit cell size along the nanowire growth direction (x direction in Figure 1). After changing the box size, the coordinates of all atoms are relaxed to obtain their equilibrium positions without any constraints except cell size. The relative longitudinal lattice constants are varied from 0.98 to 1.02. A 2% strain can be experimentally realized, for example, through epitaxial growth of a Si layer on top of a SiGe layer,[35] embedded SiGe process,[36] or depositing a capping layer such as Si_3N_4 on top of a Si layer.[36] Because the lattice constant of Ge is greater than that of Si by 4%, 2% lattice strain used in our calculations can be readily obtained by conventional strain generation methods. Wafer bending can also be an alternative method for strain generation.

In this report, we consider the [100], [110], and [111] directional hydrogen passivated SiNWs. Although surface reconstruction, chemical passivation, and cross-sectional geometry of SiNWs may have an effect on the band structure of SiNWs,[37–40] we exclude such factors and concentrate on the quantum confinement effects of SiNWs passivated with hydrogen. The structures of SiNWs are shown in Figure 1. The nearest Si−Si distances are 2.366−2.371 Å in the core region and 2.353−2.357 Å on the surface, while it is 2.364 Å in bulk Si.

The electronic band structures of SiNWs can be conjectured from the bulk band structure. It is well-known that the minimum energy point of the conduction bands and the maximum energy point of the valence bands are located near the X-point and Γ-point, respectively, which yields the indirect band gap feature of bulk Si. The conduction-band minima in silicon lie on the Δ symmetry line near the X-point, resulting in six equivalent valleys as shown in Figure 2a. These minimum points locate at $\pm$ (0.85 0 0)$2\pi/a_0$, $\pm$ (0 0.85 0)$2\pi/a_0$, and $\pm$ (0 0 0.85)$2\pi/a_0$, where a_0 is the lattice constant of bulk silicon. Iso-energy surfaces near the minima are ellipsoidal with a transverse mass of $m_t = 0.19\ m_0$ and a longitudinal mass of $m_l = 0.92\ m_0$, where m_0 is the free electron mass. The wave function of the conduction band minima near X contains a significant contribution from 3d-orbitals, and this portion of the wave function has a clearly bonding character so its energy level decreases as atomic cores are brought closer together because the energy level of a band consisting of bonding-type wave functions tends to increase with tensile strain and decrease with compressive strain.[41] In the case of a (100) thin silicon slab, biaxial in-plane tension splits the six degenerate conduction bands (Δ_6) into four higher in-plane valleys (Δ_4) and two lower out-of-plane valleys (Δ_2) as shown in Figure 2b.[36] The energy level of Δ_2 band decreases because compressive strain is

generated along the surface-normal direction by in-plane tensile strain.

The schematic feature of conduction band formation of SiNW is presented in Figure 2c. When a [100] Si nanowire is constructed along the *x*-axis, the energy level of the conduction band minima at $\pm$ (0.85 0 0)$2\pi/a_0$ are upshifted due to confinement effects (Δ_2' band) and the bands at $\pm$ (0 0.85 0)$2\pi/a_0$ and $\pm$ (0 0 0.85)$2\pi/a_0$ are folded into the Γ-point (Δ_4' band). The amount of upshift of the conduction band minima at $\pm$ (0.85 0 0)$2\pi/a_0$ is greater than those folded into the Γ-point, as shown in Figure 2d, because effective masses toward the confined directions of the conduction band minima at $\pm$ (0.85 0 0)$2\pi/a_0$ are light transverse masses. This results in [100] SiNWs having a direct band gap. Similar analogy can be applied to [110] SiNWs. In the case of [111] SiNWs, there is no conduction band minimum which can be folded into the Γ-point and thus they still exhibit an indirect band gap.

Now, we will infer the strain effects on the band structure of SiNW based on the features of bulk Si. When compressive strain is applied to [100] SiNWs toward axial direction, the energy level of the Δ_2' band decreases and that of the Δ_4' band increases, as for the biaxial tension to (100) Si slabs. This reduces the energy difference ($\Delta_2' - \Delta_4'$) due to quantum confinement and induces direct to indirect band gap change as shown in Figure 2d. Tensile strain, on the other hand, would increase the $\Delta_2' - \Delta_4'$ energy difference. Thus [100] SiNWs changes into an indirect band gap material under enough compressive axial strain and tensile strain makes the opposite tendency. Comparing the expectations based on the bulk band feature with DFT results shown below, we find that the strain dependence of conduction bands of SiNWs can be successfully understood with the bulk band feature. However, that of valence bands can not be explained with only bulk band feature because SiNWs have another valence band maximum point at the off Γ-point, which is generated by a strong quantum confinement effect in SiNWs. Thus more precise analysis should be required to explain the band structure modification induced by a lattice strain.

In Figure 3, the electronic band structures of [100] and [110] SiNWs are shown. Even though we consider SiNWs with diameters from 1 to 4 nm, our discussion will be mainly based on around 2 nm SiNWs if we do not specify the size of SiNWs and the effect of diameter variation will be addressed in the last part. When there is no lattice strain, [100] and [110] SiNWs exhibit direct band gap characteristics as expected. The band gap predicted with DFT is only 0.98 eV for the unstrained [110] SiNW, which is a well-known drawback of DFT. Zhao et al.[23] reported a band gap of 1.8 eV using the GW approximation. In spite of the discrepancy between the DFT predicted value and the experimental one, DFT results have proven useful for the prediction of trends, as shown by the numerous studies on the band gap of hydrogen-passivated nanowires without lattice strain.[23,37,42,43] On the basis of recent reports on unstrained SiNWs, we find that the trend obtained by DFT agrees well with that produced by the GW method except for the amount of band

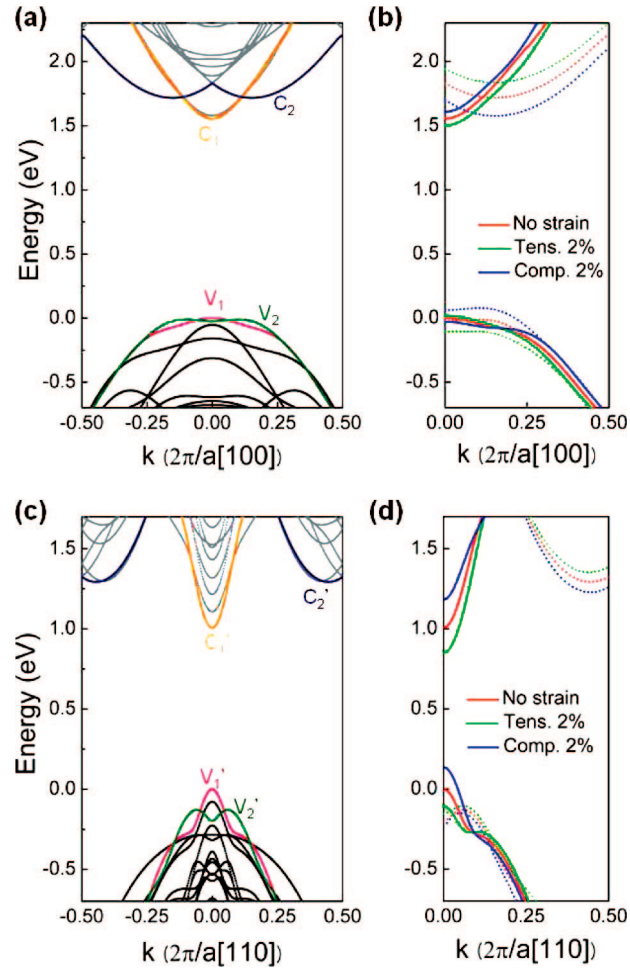

Figure 3. Electronic band structures of unstrained (a) [100] SiNWs and (c) [110] SiNWs with the effective diameter of 2.2 nm. (b,d) Strain induced band structure changes of C_1/C_1', C_2/C_2', V_1/V_1', and V_2/V_2' of [100]/[110] SiNWs. In (b) and (d), C_1, C_1', V_1, and V_1' are plotted with solid line and C_2, C_2', V_2, and V_2' with dotted line. Red color denotes the band structures of unstrained SiNWs, and green and blue colors denote those with 2% tensile and compressive strain, respectively.

gap energy.[44] Although there has been no report showing the validity of DFT method for the band structure analysis of strained SiNWs, it was reported that excited-state correction method does not make notable differences with the DFT method in the case of silicon nanoclusters.[45] Therefore, DFT can be proper method for the study of strain dependence of SiNW.

Figure 3b shows the effect of strain on the electronic structures of [100] SiNWs. Two conduction bands, C_1 and C_2, and two valence bands, V_1 and V_2, are relevant to direct-to-indirect band gap transition, where C_1 and C_2 bands are corresponding to Δ_4' and Δ_2' bands as shown in Figure 2d. C_1, C_2, and V_1 bands are consistent with the expectations based on the bulk bands, whereas the V_2 band, which has an energy maximum off Γ-point, cannot be explained with bulk bands.

In the case of [100] SiNW, the energy differences between the highest energy of the V_1 and V_2 ($\Delta V = V_1 - V_2$) and between the lowest energy of C_1 and C_2 ($\Delta C = C_2 - C_1$) are 0.01 and 0.16 eV, respectively, where a positive value of

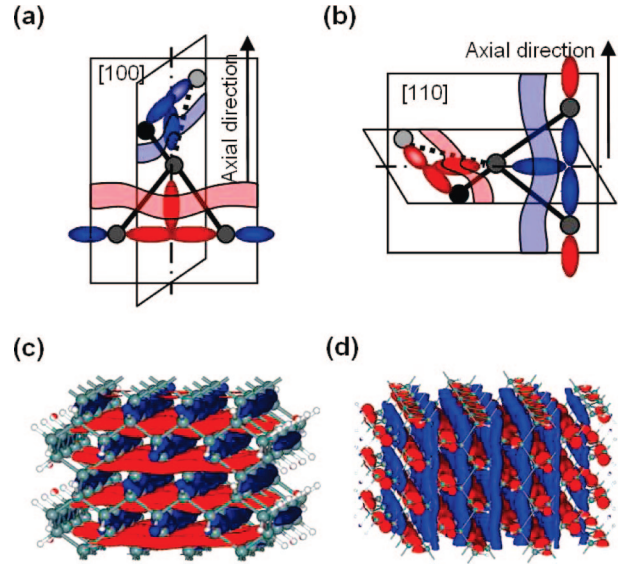

Figure 4. Schematic drawings of hybridized Si p-orbitals of (a) V_2 band of [100] SiNW and (b) V_2' band of [110] SiNW. (c) and (d) represent the wave functions of V_2 and V_2' at the Γ-point, respectively.

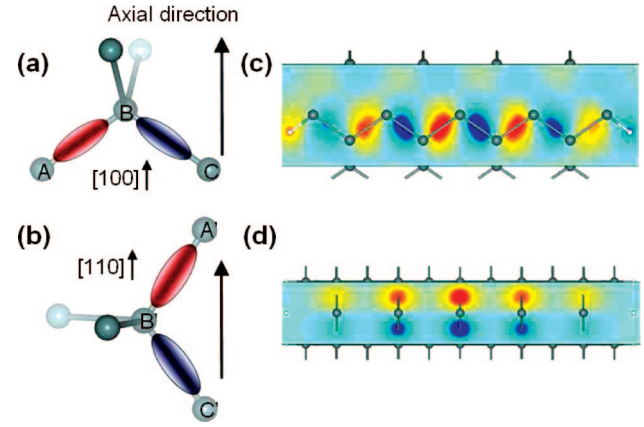

Figure 5. Schematic drawings of atomic orientations and hybridized sp^3-orbitals of (a) V_1 band of [100] SiNW and (b) V_1' band of [110] SiNW. Cross-sectional views of the wave functions of (c) V_1 and (d) V_1' bands at the Γ-point.

either ΔV (ΔC) denotes that the energy of V_1 (C_2) is higher than V_2 (C_1). If both ΔV and ΔC are positive, it implies that [100] SiNW tends to have a direct band gap. The 2% tensile strain induces changes in ΔV and ΔC into 0.11 and 0.34 eV, respectively, while 2% compressive strain results in ΔV and ΔC of −0.02 and −0.03 eV. From these, it can be concluded that a compressive strain on [100] SiNW changes the electronic band structure from a direct band gap to an indirect band gap, whereas tensile strain enhances the direct band gap characteristics of [100] SiNW.

The effect of strain on the band structure of [110] SiNWs is somewhat different from that on [100] SiNWs in that both tensile and compressive strains change the electronic band structures of [110] SiNWs from a direct band gap into an indirect band gap as shown in Figure 3d. The strain dependence of conduction bands of [110] SiNW is similar with that of [100] SiNW. The 2% compressive strain decreases the energy difference between the minimum energy of the C_2' and C_1' bands ($\Delta C' = C_2' - C_1'$) from 0.29 to 0.05 eV as like conduction bands of [100] SiNWs. Further, when 3% compressive strain is applied, $\Delta C'$ becomes negative, i.e., −0.03 eV, which implies that the band structure of [110] SiNWs is changed into the indirect band gap by compressive strain.

The different strain dependence between [110] and [100] SiNWs mainly comes from the valence bands. Energy levels of the V_2' band in a [110] SiNW increase to be higher than those of the V_1' band under tensile strain, whereas those of the V_2 band of [100] SiNW decreases. This opposite behavior of the V_2' band as compared to the V_2 band can be understood from the wave function analysis. As shown in Figure 4, the V_2 and V_2' bands arise from a linear combination of hybridized p-orbitals of Si atoms. In the case of [100] SiNWs, the wave function of V_2 expands within a confined plane ($y-z$ plane which is normal to the axial direction, as denoted in Figure 1a) and changes the phase alternately along the axial direction (Figure 4c). Therefore, there are nodal planes between positive and negative values of the wave function normal to the axial direction, which means that compression along the axial direction makes the energy of V_2 increase, and this trend can be found in the strain dependency of V_2 in Figure 3b. In the case of the V_2' band of [110] SiNWs, even though the positive (red) part of the wave function expands in a confined plane like V_2, the negative (blue) part of the wave function expands along the axial direction (Figure 4d). Thus, there is no nodal plane along the axial direction, causing a different strain dependence of the V_2' band.

The V_1' band responds to a strain more sensitively, and its strain dependence is opposite to that of the V_1. When the axial strain is varied from 2% compressive strain to 2% tensile strain, the highest energy of the V_1' band decreases by 0.24 eV, whereas that of the V_1 band increases by 0.05 eV. This difference can also be explained through wave function analysis of V_1 and V_1' bands. The wave functions of V_1 and V_1' at the Γ-point have the feature of an sp^3-hybrid bonding type as shown in Figure 5. The wave function of V_1' band has nodal planes in the confined plane along the axial direction ($x-z$ or $x-y$ plane), whereas the nodal planes of the V_1 band are perpendicular to the axial direction ($y-z$ plane). When the axial tensile strain is applied, the distance between Si atoms at A′ and C′ positions of the [110] SiNW (Figure 5b) lengthens by the same amount of applied strain, whereas the distance between Si atoms at A and C of the [100] SiNW (Figure 5a) shortens by only 20% of the amount of applied axial lattice strain, which can be interpreted as a Poisson ratio. Thus, under tensile stress, the V_1' bands are stabilized and the energy decreases, while the V_1 bands are slightly destabilized and the energy increases by a smaller amount than that of V_1'. Hence, the different strain dependence of [110] SiNWs from [100] SiNWs can be attributed that the energy level of V_1' becomes lower than that of V_2' as tensile strain increases in the case of [110] SiNWs, while the energy level of V_1 is still higher than that of V_2 under tensile strain.

SiNWs with high index plane tend to have an indirect band gap.[25] Because the conduction band minimum of bulk Si

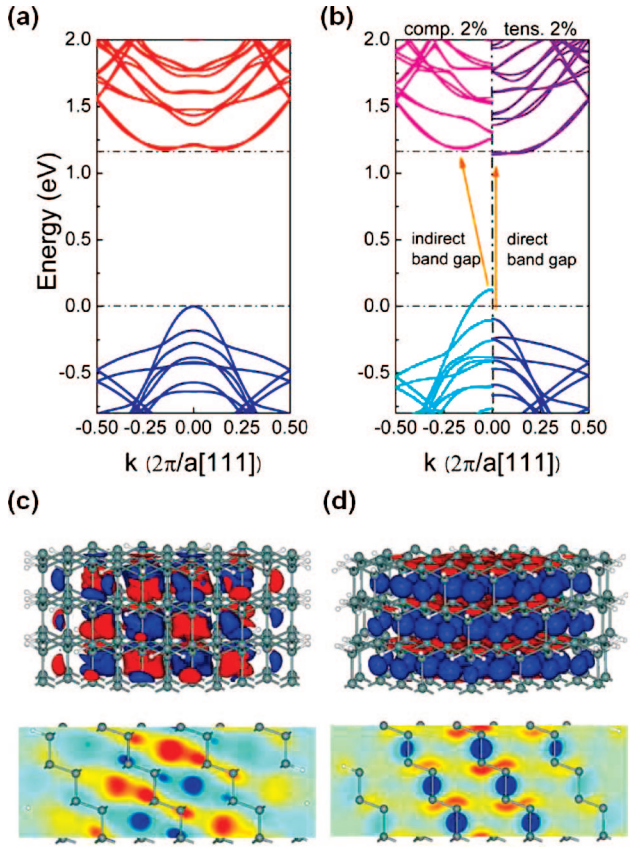

Figure 6. Electronic band structure of [111] SiNW with a diameter of 2.1 nm: (a) unstrained and (b) 2% compressive (negative *k*-vectors) and tensile (positive *k*-vector) strain. The wave functions of the conduction band minimum and the valence band maximum at the Γ-point are shown in (c) and (d), respectively. Lower parts of (c) and (d) are the cross-sectional views of each wave function.

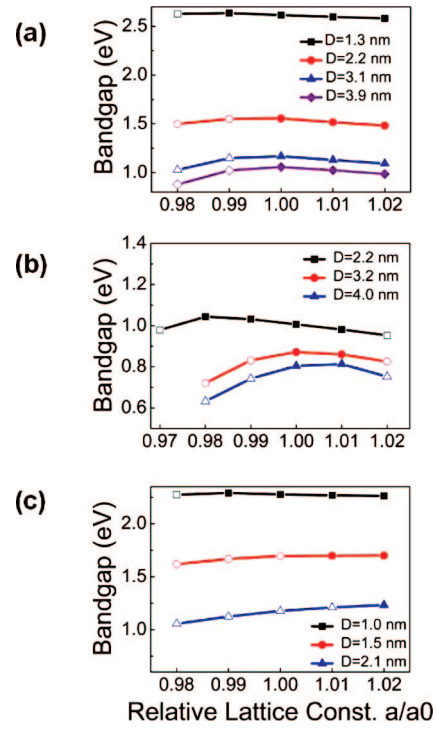

Figure 7. Variation of a band gap with regard to diameters and relative lattice constants of (a) [100], (b) [110], and (c) [111] SiNWs. Filled and unfilled symbols denote the direct and indirect band gap, respectively.

(Figure 2a) cannot be folded into the Γ-point of high index plane SiNWs, the conduction band minimum of nanowire is off from the Γ-point and thereby yields an indirect band gap. [111] SiNWs have also an indirect band gap even at diameters as small as 1.5 nm. The electronic band structure of [111] SiNW with a diameter of 2.1 nm is plotted in Figure 6. The conduction band minimum locates at the position of $0.3 \times 2\pi/a[111]$ and the valence band maximum does so at the Γ-point. In the valence bands, there are no p-orbital hybridized bands such as the V_2 band in [100] or the V_2' band in [110] SiNWs because the directions of hybridized p-orbitals lie oblique to the axial direction.

Because there are no V_2 or V_2' bands in [111] SiNWs, it can be expected that tensile strain is helpful to make [111] SiNWs exhibit a direct band gap as discussed above. The variations of the electronic band structure of [111] SiNW at 2% tensile and compressive strain are represented in Figure 6b. It shows that the compressive strain enhances the indirect band gap tendency, whereas the tensile strain drives [111] SiNWs to have a direct band gap. This result shows that our expectation based on the analyses for [100] and [110] SiNWs can be applicable to predict the strain induced band structure change of [111] SiNWs. Figure 6b shows that the minimum energy of the conduction band (CB) and the maximum energy of the valence band (VB) at the Γ-point increase under compressive strain. This is attributed to the characteristics of each wave function of their bands. As shown in Figure 6c,d, the wave functions of both the CB and VB bands have nodal planes (within $y-z$ planes) along the x-axial direction and the antibonding character makes the energy of these bands increase with compressive strain.

Finally, we discuss the diameter dependence of [100], [110], and [111] SiNWs on the uniaxial strain. We vary the diameters of SiNWs from 1 to 4 nm and the strength of strain. On these variations, we calculate the band gap energies and ascertain whether the band gap is direct (filled symbols) or indirect (unfilled symbols) as shown in Figure 7.

As the diameter of SiNWs becomes smaller, there are several notable features induced by quantum confinement: (1) The band gap tends to be larger. (2) Larger quantum confinement effect increases the tendency to have a direct band gap. (3) The variation of band gap energy with the lattice strain is reduced. The band gap energy of 1.3 nm sized [100] SiNW changes by 0.05 eV and that of 4.0 nm diameter sized SiNW is 0.19 eV when the lattice strain changes from 2% compressive strain to 2% tensile strain.

Although [100] SiNWs exhibit a direct band gap, only 1% axial compressive strain induces a transition to an indirect band gap when the diameter is larger than 2 nm as shown in Figure 7a. The weakness for compressive strain originates from the small $\Delta_2' - \Delta_4'$ energy difference (ΔC) as shown in Figure 3. Although we do not show the ΔC variation with diameters of SiNWs, it is found that ΔC decreases as the diameter increases. When the diameter changes from 2.2 to

4.0 nm, ΔC decreases from 0.16 to 0.08 eV. This implies that larger [100] SiNWs are much easier to exhibit an indirect band gap characteristic under very small lattice strain.

The strain dependence of [110] SiNW is unique in that both tensile and compressive strain drives a direct to indirect band gap change and such dependence gets stronger as the diameter becomes larger. When the diameter of [110] SiNWs is greater than 3.2 nm, a direct band gap appears between unstrained and 1% tensile strained SiNWs as shown in Figure 7b. Like [100] SiNWs, [110] SiNWs have weak resistance to compressive strain because of small energy difference between the C_1' and C_2' bands. Thus, the amount of lattice strain has to be carefully controlled between strain-free and 1% tensile strain for [110] SiNWs when the diameter is greater than 3 nm.

In the case of [111] SiNWs, they have an indirect band gap even at the unstrained 1.5 nm sized nanowire. As the diameter becomes smaller, the magnitude of the tensile lattice strain to make indirect to direct band gap change decreases. A 2% tensile strain is necessary to have a direct band gap when the diameter is 2.1 nm, whereas only 1% tensile strain is enough when the diameter is 1.5 nm.

In summary, we investigate the electronic band structures of [100], [110], and [111] SiNWs without and with lattice strain using density functional theory. We show that the band structures can be manipulated to have direct band gaps by applying lattice strain. We also present that the transition between direct and indirect band gap of SiNW due to lattice strain is strongly dependent on the crystal directions, the diameters of SiNWs, and the strength of strain. For each SiNW under study, compressive strain leads to indirect band gap characteristics. On the other hand, the effects of tensile strain are different with respect to the crystal orientations. Tensile strain enhances the direct band gap characters of [100] and [111] SiNWs, whereas it drives [110] SiNWs to have an indirect band gap. The origin of this different strain dependence on crystal orientations is attributed to the characteristics of bonding type and shapes of wave functions of the valence bands. We also discussed the size dependence. As the diameter becomes smaller, quantum confinement effects become dominant and the significance of the lattice strain to make direct band gap reduces.

We expect that engineering the lattice strain can be an effective way for controlling the electronic band structure of SiNWs and thus shall be a useful tool for designing nanophotonic and electronic devices using SiNWs.

Acknowledgment. We thank Dr. Jung Hoon Lee (KIST) and Prof. Hyung Joon Choi (Yonsei University) for helpful discussions.

References

(1) Cui, Y.; Zhong, Z.; Wang, D.; Wang, W. U.; Lieber, C. M. *Nano Lett.* **2003**, *3*, 149.
(2) Wang, Y.; Lew, K.-K.; Ho, T.-T.; Pan, L.; Novak, S. W.; Dickey, E. C.; Redwing, J. M.; Mayer, T. S. *Nano Lett.* **2005**, *5*, 2139.
(3) Yang, C.; Barrelet, C. J.; Capasso, F.; Lieber, C. M. *Nano Lett.* **2006**, *6*, 2929.
(4) Cui, Y.; Wei, Q. Q.; Park, H. K.; Lieber, C. M. *Science* **2001**, *293*, 1289.
(5) Wu, Y.; Cui, Y.; Huynh, L.; Barrelet, C. J.; Bell, D. C.; Lieber, C. M. *Nano Lett.* **2004**, *4*, 433.
(6) Yang, C.; Zhong, Z.; Lieber, C. M. *Science* **2005**, *310*, 1304.
(7) Suk, S. D.; Lee, S.-Y.; Kim, S.-M.; Yoon, E.-J.; Kim, M.-S.; Li, M.; Oh, C. W.; Yeo, K. H.; Kim, S. H.; Shin, D.-S.; Lee, K.-H.; Park, H. S.; Han, J. N.; Park, C. J.; Park, J.-B.; Kim, D.-W.; Park, D.; Ryu, B.-I. *Proc. Electron Devices Meet.* **2005**, 735.
(8) McAlpine, M. C.; Friedman, R. S.; Jin, S.; Lin, K.-h.; Wang, W. U.; Lieber, C. M. *Nano Lett.* **2003**, *3*, 1531.
(9) Zhong, Z.; Fang, Y.; Lu, W.; Lieber, C. M. *Nano Lett.* **2005**, *5*, 1143.
(10) Wang, D.; Sheriff, B. A.; Heath, J. R. *Nano Lett.* **2006**, *6*, 1096.
(11) Green, M. A.; Zhao, J.; Wang, A.; Reece, P. J.; Gal, M. *Nature* **2001**, *412*, 805.
(12) Ng, W. L.; Lourenco, M. A.; Gwilliam, R. M.; Ledain, S.; Shao, G.; Homewood, K. P. *Nature* **2001**, *410*, 192.
(13) Hirschman, K. D.; Tsybeskov, L.; Duttagupta, S. P.; Fauchet, P. M. *Nature* **1996**, *384*, 338.
(14) Almeida, V. R.; Barrios, C. A.; Panepucci, R. R.; Lipson, M. *Nature* **2004**, *431*, 1081.
(15) Wilson, W. L.; Szajowski, P. F.; Brus, L. E. *Science* **1993**, *262*, 1242.
(16) Canham, L. T. *Appl. Phys. Lett.* **1990**, *57*, 1046.
(17) Guichard, A. R.; Barsic, D. N.; Sharma, S.; Kamins, T. I.; Brongersma, M. L. *Nano Lett.* **2006**, *6*, 2140.
(18) Kovalev, D.; Heckler, H.; Ben-Chorm, M.; Polisski, G.; Schwartzkopff, M.; Koch, F. *Phys. Rev. Lett.* **1998**, *81*, 2803.
(19) Castagna, M. E.; Coffa, S.; Monaco, M.; Caristia, L.; Messina, A.; Mangano, R.; Bongiorno, C. *Physica E* **2003**, *16*, 547.
(20) Huo, J; Solanki, R; Freeouf, J. L.; Carruthers, J. R. *Nanotechnology* **2004**, *15*, 1848.
(21) Li, C. P.; Sun, X. H.; Wong, N. B.; Lee, C. S.; Lee, S. T.; Teo, B. K. *Chem. Phys. Lett.* **2002**, *365*, 22.
(22) Lyons, D. M.; Ryan, K. M.; Morris, M. A.; Holmes, J. D. *Nano Lett.* **2002**, *2*, 811.
(23) Zhao, X.; Wei, C. M.; Yang, L.; Chou, M. Y. *Phys. Rev. Lett.* **2004**, *92*, 236805.
(24) Read, A. J.; Needs, R. J.; Nash, K. J.; Canham, L. T.; Calcott, P. D. J.; Qteish, A. *Phys. Rev. Lett.* **1992**, *69*, 1232.
(25) Scheel, H.; Reich, S.; Thomsen, C. *Phys. Status Solidi B* **2005**, *242*, 2474.
(26) Cui, Y.; Lauhon, L. J.; Gudiksen, M. S.; Wang, J.; Lieber, C. M. *Appl. Phys. Lett.* **2001**, *78*, 2214.
(27) Schmidt, V.; Senz, S.; Gosele, U. *Nano Lett.* **2005**, *5*, 931.
(28) Fischetti, M. V.; Laux, S. E. J. *Appl. Phys. Lett.* **1996**, *80*, 2234.
(29) Uchida, K.; Krishnamohan, T.; Saraswat, K. C.; Nishi, Y. *Proc. Electron Devices Meet.* **2005**, 135.
(30) Thompson, S. E.; Sun, G.; Choi, Y. S.; Nishida, T. *IEEE Trans. Electron Devices* **2006**, *53*, 1010.
(31) Audoit, G.; Mhuircheartaigh, É. N.; Lipson, S. M.; Morris, M. A.; Blau, W. J.; Holmes, J. D. *J. Mater. Chem.* **2005**, *15*, 4809.
(32) (a) Kresse, G.; Hafner, J. *Phys. Rev. B* **1994**, *49*, 14251. (b) Kresse, G.; Furthmuller, J. *Comput. Mater. Sci.* **1996**, *6*, 15.
(33) Blochl, P. E. *Phys. Rev. B* **1994**, *50*, 17953.
(34) Soler, J. M.; Artacho, E.; Gale, J. D.; García, A.; Junquera, J.; Ordejón, P.; Sánchez-Portal, D. *J. Phys.: Condens. Matter* **2002**, *14*, 2745.
(35) Bean, J. C. *Science* **1985**, *230*, 127.
(36) Liu, C. W.; Maikap, S.; Yu, C.-Y. *IEEE Circuits Devices Mag.* **2005**, *21*, 21.
(37) Singh, A. K.; Kumar, V.; Note, R.; Kawazoe, Y. *Nano Lett.* **2006**, *6*, 920.
(38) Yeh, C. Y.; Zhang, S. B.; Zunger, A. *Phys. Rev. B* **1994**, *50*, 14405.
(39) Singh, A. K.; Kumar, V.; Note, R.; Kawazoe, Y. *Nano Lett.* **2005**, *5*, 2302.
(40) Leu, P. W.; Shan, B.; Cho, K. *Phys. Rev. B* **2006**, *73*, 195320.
(41) Chidambaram, P. R.; Bowen, C.; Chakravarthi, S.; Machala, C.; Wise, R. *IEEE Trans. Electron Devices* **2006**, *53*, 944.
(42) Nolan, M.; O'Callaghan, S.; Fagas, G.; Greer, J. C.; Frauenheim, T. *Nano Lett.* **2007**, *7*, 34.
(43) Vo, T.; Williamson, A. J.; Galli, G. *Phys. Rev. B* **2006**, *74*, 045116.
(44) (a) Yang, L.; Spataru, C. D.; Louie, S. G.; Chou, M. Y. *Phys. Rev. B* **2007**, *75*, 201304. (b) Yan, J.-A.; Yang, L.; Chou, M. Y. *Phys. Rev. B* **2007**, *76*, 115319.Chou and co-workers reported the electronic band structures of 1 nm sized [110] SiNW, using both DFT and GW calculations. When we compare these results, we find that the electronic band structures of DFT show good agreements with GW results except the band gap and valence band width. The DFT predicted band gap is 1.9 eV smaller than GW predicted one.
(45) Peng, X.-H.; Ganti, S.; Alizadeh, A.; Sharma, P.; Kumar, S. K.; Nayak, S. K. *Phys. Rev. B* **2006**, *74*, 035339.

NL0734140